Applied Catalysis A: General 528 (2016) 74–85

Contents lists available at ScienceDirect

Applied Catalysis A: General

journal homepage: www.elsevier.com/locate/apcata

NiMoS HDS catalysts – The effect of the Ti and Zr incorporation into the silica support and of the catalyst preparation methodology on the orientation and activity of the formed MoS_2 slabs

Alano Viera da Silva Neto[a], Edson Roberto Leite[b], Victor Teixeira da Silva[c], José Luiz Zotin[d], Ernesto Antonio Urquieta-González[a,*]

[a] Laboratory of Adsorption and Applied Catalysis, Research Center on Advanced Materials and Energy, Sao Carlos Federal University, C. Postal 676, CEP 13565-905, São Carlos, SP, Brazil
[b] Nucleus of Innovation, Research Center on Advanced Materials and Energy, São Carlos Federal University, C. Postal 676, CEP 13565-905, Sao Carlos, SP, Brazil
[c] Universidade Federal do Rio de Janeiro, COPPE, Av. Horácio Macedo, 2030-101, Cidade Universitária, CEP 21941-450, Rio de Janeiro, RJ, Brazil
[d] Cenpes/Petrobras, Av. Horácio Macedo 950, Ilha do Fundão, Rio de Janeiro, RJ, Brazil

ARTICLE INFO

Article history:
Received 25 May 2016
Received in revised form
16 September 2016
Accepted 27 September 2016
Available online 28 September 2016

Keywords:
SiO_2
SiO_2-TiO_2
SiO_2-ZrO_2
NiMoS catalysts
MoS_2 slabs
Crystal orientation
Thiophene HDS

ABSTRACT

HDS NiMo catalyst precursors supported on SiO_2, SiO_2-TiO_2 or SiO_2-ZrO_2, having high specific surface areas and highly dispersed Mo species were prepared using a one-pot sol-gel methodology or by wet impregnation. After the catalyst precursor sulfidation, HRTEM and Raman analyses evidenced the effective formation of MoS_2 slabs on the support. For the NiMoS-Si catalyst (precursor one-pot synthesized), there was a high formation of edge-bonded oriented MoS_2 slabs, whereas for the NiMoS/Si prepared by impregnation, basal-bonded MoS_2 slabs were more abundant. Coherent with the formation of MoS_2 slabs and the promoting effect of Ni, all of the prepared NiMoS catalysts were active in the HDS of thiophene, with those one-pot supported on SiO_2 or SiO_2-ZrO_2 being the most active. Due to the strong interaction between Mo and Ti, the NiMoS-SiTi catalyst did not show consistent formation of MoS_2 slabs and consequently it presented the lowest activity. No observable effect in the HDS activity of the Zr incorporation into the SiO_2 framework was noticed. The considerable specific activity (SA) of the catalysts NiMoS-Si and NiMoS/Si, was respectively related to the formation of the most active edge-bonded MoS_2 slabs and to the well-active Type II HDS catalysts on multilayer basal-bonded MoS_2 slabs. The studied NiMoS-Si and NiMo-SiZr with high SA values evidences that the one-pot sol-gel synthesis methodology used to prepare the catalyst precursor leads to highly active HDS catalysts with the important advantages of reducing the preparation time, energy consumption, and consequently diminishing the catalyst production cost.

1. Introduction

The growing demand for high performance fuels associated with highly restrictive environmental laws have imposed rigorous constraints and led to the optimization of the hydrotreatment processes in petroleum refineries to produce fuels with extremely low levels of precursor pollutants such as sulfur organic compounds [1,2]. The conventional removal of sulfur from petroleum fuels is carried out by the well-known hydrodesulfurization process (HDS), in which the oil fractions react with hydrogen under severe operational conditions and in the presence of a catalyst producing sulfidric acid and sulfur free compounds [1,2].

The commercial HDS catalysts usually consist of Mo sulfides promoted with Co or Ni sulfides supported on γ-alumina [1]. There is a constant search for more active catalysts which may involve the use of new active phases, additives, new carriers or combination of them [3–5]. Regarding new supports, a challenge is to obtain solids with high specific surface area allowing high dispersion of the active phase in adequate interaction with the carrier surface. Thus, aiming to improve the mentioned properties, new supports such as SiO_2 [6], MgO [7], ZrO_2 [8], TiO_2 [9], zeolites [10], mesoporous materials [11,12] and carbon nanotubes [12] have been studied. ZrO_2 [13] and TiO_2 [14] have been used as HDT catalyst carriers, and sulfided catalysts with higher intrinsic activity have been obtained by some research groups [13–15]. However, ZrO_2 and TiO_2 have

* Corresponding author.
E-mail addresses: ernesto.urquieta@gmail.com, urquieta@ufscar.br (E.A. Urquieta-González).

http://dx.doi.org/10.1016/j.apcata.2016.09.019
0926-860X/

low specific surface area and pore volume and limited thermal stability that have restricted their application. Mixed oxides such as Al_2O_3-ZrO_2 [16,17], TiO_2-Al_2O_3 [18], ZrO_2-SiO_2 [19] and TiO_2-SiO_2 [20,21], or ordered mesoporous silicas as MCM-41 [22], HMS [23] or SBA-15 [24], with isomorphically substituted Ti [25] or Zr [11], have been proposed as support for HDT catalysts in order to overcome those limitations.

As pointed out, besides of the physicochemical properties of the support which determine the interaction with metal precursors and the dispersion of the active phase, the textural properties, as porosity and pore volume, have an important role in the activity of the HDS catalysts. Several methods have been used to synthesize supports with improved textural properties. The sol-gel methodology with its well-known advantages as purity, homogeneity, and tunable porosity of the obtained materials, as well as the possibility of preparing materials with high specific surface areas at low temperatures [26], has been highly used. High specific surface area Al_2O_3 [27], SiO_2 [28], TiO_2 [29], ZrO_2 [30], TiO_2-Al_2O_3 [31], SiO_2-Al_2O_3 [32] or ZrO_2-TiO_2 [33] supports have been synthesized by sol-gel and have shown better performance and thermal stability than when prepared by precipitation or co-precipitation.

The sol-gel method is a process in which a solution or sol undergoes to a transition state and becomes a rigid mass (gel). This is a multistep procedure involving chemical and physical steps associated with the hydrolysis and polycondensation of organometallic or inorganic precursors, drying, and densification. Basically, it is used in a homogeneous three-component system: a precursor of the metallic oxide, a solvent, and an acid or basic catalyst. The most commonly used precursors are metal alkoxides M(OR)n, such as alkoxysilanes ($Si(OR)_4$): tetramethoxysilane (TMOS) and tetraethoxysilane (TEOS) [34,35] or aluminum isopropoxide, zirconium propoxide or titanium tetraisopropoxide [36,37].

In order to tune the porosity and the pore volume of the final desired support, an organic template may be also added into the sol-gel mixture. In this sense, citric acid has been satisfactorily used, with the size and volume of the generated mesopores, linearly increasing with the amount of citric acid added and, consequently, also increasing the specific surface area of the formed solid [38]. Therefore, oxides or mixed oxides prepared by sol-gel, such as SiO_2, SiO_2-TiO_2 or SiO_2-ZrO_2 could be versatile materials to be used as catalyst support, as their textural properties could be tailored [37–39]. It is also claimed by several authors [38,40–43] that during the sol-gel preparation, the presence of citric acid in the sol mixture promotes the dispersion of the metallic species due to their ability to chelate metal ions. On the other hand, it has also been reported that the addition of chelating ligands such as citric acid to the impregnating solution has a beneficial effect on the activity of the HDS catalysts [41,44,45]. The improved activity has been ascribed to a better dispersion of nickel (or cobalt) and molybdenum on the support and to a higher sulfidation temperature of those promoters (Ni or Co) when compared with catalysts prepared without a chelating agent [46]. Both factors would enhance the formation of the so-called Ni–Mo–S type II active sites [47], which are considered the best active phase in hydrotreatment catalysts [7].

On the other hand, as an alternative to the conventional catalyst preparation by impregnation, it has recently been quite applied the addition of the metallic precursor salts into the sol mixture used in the sol-gel preparation of the support [17,30,43]. This one-pot methodology reduces the synthesis steps and it has been claimed that the obtained catalyst precursors present the active metallic species better dispersed [48].

Taking into consideration the above discussion, the purpose of the present work was to prepare silica, silica-titania and silica-zirconia supported NiMo oxides, the precursors of HDS NiMoS catalysts, by a one-pot sol-gel methodology and to compare their properties with similar catalysts prepared by wet impregnation with a chelating agent on the corresponding carriers. HDS of thiophene was used as a model reaction for evaluating the catalytic activity of the sulfided catalysts. Atomic absorption spectroscopy (AAS), Energy-dispersive X-ray spectroscopy (EDS), nitrogen physisorption, X-ray diffraction (XRD), temperature programmed reduction by hydrogen (H_2-TPR), UV–vis diffuse reflectance spectroscopy (UV–vis DRS), High resolution transmission electronic microscopy (HRTEM) and Raman spectroscopy were used to sample characterization.

2. Experimental

2.1. Synthesis by a sol-gel methodology of silica, silica-titania and silica-zirconia pure supports and of supported NiMo oxides

The silica, silica-titania and silica-zirconia pure supports were obtained by a sol-gel synthesis methodology using a Si/Me ratio of 10 (Me = Ti or Zr), tetraethylorthosilicate, zirconium propoxide, titanium isopropoxide, ethanol and citric (CA) and nitric acids. The composition of the resultant sol mixture was: Si: 0.1Ti(Zr): $4H_2O$: 6EtOH: yCA, with $y = 1$ or 3 for the synthesis of pure silica or the mixed oxides, respectively. The sol mixture was dried at 70 °C for 72 h and the obtained gel calcined in static air at 550 °C during 2.5 h.

The supported NiMo oxides, the precursors of the supported silica, silica-titania and silica-zirconia NiMoS catalysts, were prepared adding the necessary amount of Ni and Mo salts in the sol mixture of the respective support to generate solids with 3 wt% of NiO and 12 wt% of MoO_3 (one-pot synthesis methodology). For comparison purposes, precursors of the catalysts with the same composition were prepared by wet impregnation using a mixture containing citric acid (chelating agent), ammonium heptamolybdate and nickel nitrate (CA/Mo mole ratio = 1), being subsequently dried and calcined in the same conditions defined above. The corresponding supported NiMo oxides were denominated as NiMo(ox)-Si; NiMo(ox)-SiTi; NiMo(ox)-SiZr when the one-pot procedure was used or as NiMo(ox)/Si; NiMo(ox)/SiTi; NiMo(ox)/SiZr when prepared by wet impregnation.

2.2. Pure supports, catalyst precursors and NiMoS catalysts characterization

The chemical composition of the catalyst precursors was obtained by atomic absorption spectroscopy (AAS) analyses that were carried out in a Perkin Elmer 5000 series spectrometer. Chemical analyses of the supports for the determination of the composition of Ti and Zr were also performed by EDS using an electron microscope FEI Magellan L 400, operating at 15 V of acceleration voltage. Supports and the catalyst precursors were characterized by powder X-ray diffraction (XRD) in a Shimadzu DRX-600 spectrometer using a CuKα radiation (λ = 1.5406 Å). The textural properties of the supports and the catalyst precursors were determined from N_2 adsorption/desorption isotherms obtained at −196 °C K on an ASAP 2020 Micromeritics equipment. Prior to sorption experiments, the samples were degassed under vacuum at 190 °C during 2 h. The UV–vis diffuse reflectance spectra (UV-vis DRS) of supports and catalyst precursors were recorded at room temperature using a Varian Cary 5G spectrometer and barium oxide as a reference material. The H_2-TPR experiments were carried out in a Micromeritics Pulse Chemisorb 2920 analyzer with the samples being previously treated under nitrogen flow at 200 °C during 30 min. The measurements were performed from room temperature to 1000 °C using a heating rate of 10 °C min^{-1} and a H_2 flow (10% V/V in N_2). HRTEM images of the sulfided catalysts were obtained using a FEI TECNAI F20 microscope operating at 200 kV. Raman spectra of the sulfided catalysts were obtained in a Horiba Jobin-Yvon Raman micro-

Table 1
Chemical composition[a] and textural properties of the pure supports and NiMo(ox) catalyst precursors.

Sample	TiO_2[b] (wt%)	ZrO_2[b] (wt%)	MoO_3[c] (wt%)	NiO[c] (wt%)	A_{BET}[e] (m^2g^{-1})	Vp (cm^3g^{-1})	Dp (nm)
SiO_2	–	–	–	–	963	1.5	6.0
SiO_2-TiO_2	11.5 (11.7)	–	–	–	822	1.4	6.4
SiO_2-ZrO_2		17 (17.5)	–	–	731	0.9	4.4
NiMo(ox)-Si	–	–	10 (12)	2.5 (3)	674	0.8	4.6
NiMo(ox)-SiTi	–	–	10 (12)	2.5 (3)	549	1.0	7.8
NiMo(ox)-SiZr	–	–	10.5 (12)	2.4 (3)	524	0.9	7.0
NiMo(ox)/Si	–	–	11 (12)	2.5 (3)	437	0.8	6.0
NiMo(ox)/SiTi	–	–	11 (12)	2.5 (3)	367	0.3	5.0
NiMo(ox)/SiZr	–	–	12 (12)	2.5 (3)	368	0.4	4.0
NiMoP(ox)/Al_2O_3[d]	–	–	18.8	5.2	–	–	–

[a] In parenthesis is shown the nominal value.
[b] Determined by EDS.
[c] Determined by AAS.
[d] Supplied by the manufacturer.
[e] Textural properties were determined from N_2-adsorption/desorption isotherms at −196 °C.

spectrometer LabRAM at room temperature using the 633 nm line of a 5.9 mW He–Ne laser as the excitation source through an Olympus TM BX41 optical microscope. The NiMoS catalysts analyzed by HRTEM and Raman spectroscopy were sulfided by the same procedure described in the following section 2.3.

2.3. Hydrodesulfurization activity

The activity of the NiMoS catalysts was evaluated using the hydrodesulfurization of thiophene as a model reaction. Samples of the studied catalysts and the reference commercial one were previously separated on a 100 mesh sieve. The reaction was carried out in the vapor phase using a fixed-bed microreactor operated under continuous flow at 240, 260, 280 or 300 °C. To generate the sulfided NiMoS catalysts, an amount of 100 mg of each catalyst precursor was placed inside of the quartz reactor and subsequently sulfided at 673 K during 2 h under a flow of 30 ml min^{-1} of H_2S (5% V/V in H_2). The reactor feed was constituted by a mixture of 8.2% of thiophene in H_2 (V/V) generated by passing 20 ml min^{-1} of H_2 through liquid thiophene in a saturator at 20 °C and at atmospheric pressure. The conversions of thiophene were kept below 20% to operate in differential regime. The reactor effluent was analyzed online by gas chromatography using a Micro-GC Varian CP 4900 gas chromatograph equipped with a TDC detector and a CP-5CB module column.

The thiophene conversion (X_T) to hydrodesulfurized products was calculated using Eq. (1), where x_{iDS} is the molar fraction of the hydrodesulfurized product i and x_{Th} the molar fraction of the non-reacted thiophene.

$$X_T = 100 \times \left(\sum x_{iDS} / (x_{Th} + \sum x_{iDS}) \right) \quad (1)$$

The specific activity (SA) to the HDS of thiophene of the supported NiMoS studied catalysts in the used heterogeneous reactor working at steady-state conditions was calculated according to Eq. (2) [17,49].

$$SA = [X \times F] / m \quad (2)$$

where X is the conversion of thiophene (Eq. (1)), F is the molar flow of thiophene (mol s^{-1}) fed to the reactor, and m refers to the metal mols of the used catalyst (mol_{Me}), with $mol_{Me} = (mol_{Mo} + mol_{Ni})$.

3. Results and discussion

3.1. Pure supports and catalyst precursors

Table 1 shows the chemical composition related with the Ti and Zr oxides in the SiTi and SiZr mixed oxides and of Mo and Ni oxides in the catalyst precursors. As it can be seen, the experimental values are approximately close to the nominal ones and the differences are attributed to the inherent errors of the analytical procedures.

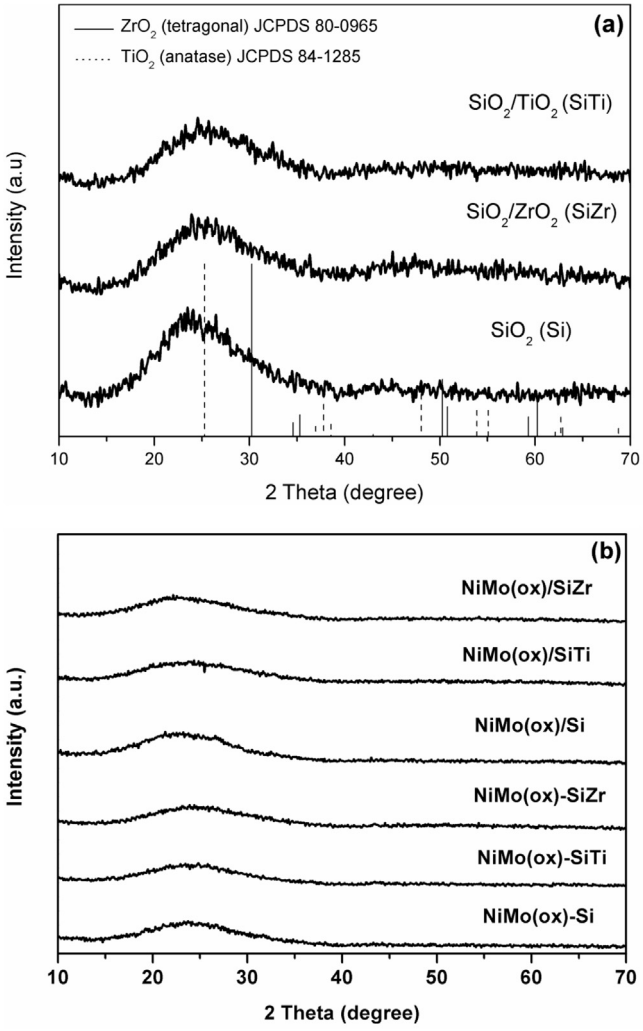

Fig. 1. XRD diffractograms of: (a) silica, silica-zirconia and silica-titania pure supports; (b) supported NiMo oxides.

XRD patterns of the silica, silica-titania and silica-zirconia pure supports and of the NiMo catalyst precursors prepared by the one pot or impregnation procedures are shown in Fig. 1a and b, respectively. It can be seen from Fig. 1a that the diffractograms of the

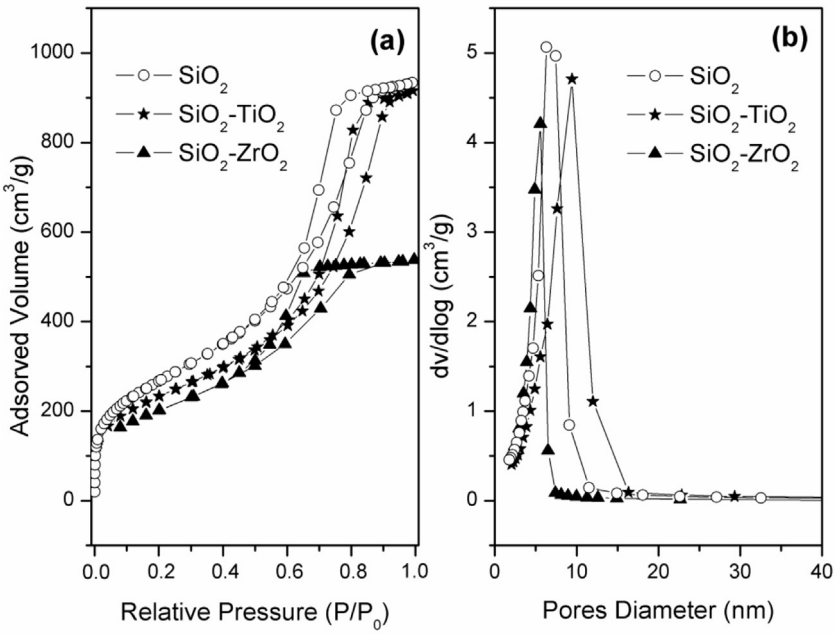

Fig. 2. Pure supports: (a) N_2 adsorption-desorption isotherms; (b) Pore size distribution curves.

supports constituted by mixed oxides do not show the presence of any crystalline phase related to TiO_2 or ZrO_2 oxides. This result could indicate that most of the Ti and Zr species are highly dispersed in the amorphous silica framework, forming homogeneous linkages of Ti-O-Si or Zr-O-Si [37,50,51]. This high degree of mixing is an evidence of the promoting effect of the citric acid acting as complexing agent, decreasing the hydrolysis and condensation rates of the Zr and Ti alkoxides, which are much faster than that of the silicon alkoxide, hence favoring the formation of highly homogeneous mixed oxides [36,37].

The XRD patterns of the catalyst precursors (Fig. 1b) did not show any diffraction of crystalline phases related to Mo and Ni oxides, indicating that most of these species must be present as very small particles highly dispersed on the supports [52,53]. Similar behavior was also observed by Zepeda et al. [54,55] and Gutiérrez et al. [56], who respectively prepared supported Mo and CoMo oxides on HMS modified with Ti or supported Mo and NiMo oxides on SBA-15 and SBA-15 modified with ZrO_2.

All of the pure supports (Fig. 2a) and catalyst precursors (Fig. 3) exhibited typical type IV isotherms, which are characteristics of mesoporous materials. The similarity of the H2 hysteresis loop with the H2 type, at relative pressure between 0.4 and 0.8, indicates the presence of ink bottle type pores in these materials [37,57].

As it can be seen from Table 1, the pure silica presents a specific surface area (A_{BET}) of 963 m^2/g, that is a consequence of the use of citric acid as pores template. The formation of pores in the sol-gel synthesis of silica using citric acid was described by Takahashi et al. [38,57]. According to these authors, the citric acid interacts with the silica species by weak hydrogen bonds occupying spaces inside the structure of the support. Citric acid decomposes at a relatively high temperature, allowing the retention of a large number of siloxane bonds and minimizing shrinkage of the silica structure during heating. After citric acid decomposition, the space previously occupied results in a large number of pores with a relative homogenous distribution sizes. This preparation route is possible because citric acid has high solubility in water and ethanol, small crystallization tendency from aqueous solution, weak interaction with the silica surface, and high decomposition temperature.

In comparison with pure silica, from Table 1 it is noticeable that the specific surface area and porous volume of the silica-titania and silica-zirconia supports decreased, but reaching values higher than 700 m^2/g. As reported by Wu et al. [36,51], that decrease is attributed to the incorporation of Zr and Ti into the silica framework, which results in the formation of Si-Ti or Si-Zr mixed oxides with a composite texture constituted by compact and cross-linked clusters generated from Si-O-Ti and Si-O-Zr linkages. Confirming the behavior described by Wu et al. [36,50], the XRD diffractogram of the studied SiTi or SiZr supports (Fig. 1a) do not show any crystalline phases related to TiO_2 or ZrO_2. The pore size distributions of the pure supports (Fig. 2b) are relatively narrow, a fact that it is also attributed to the use of citric acid as pores template [57].

As it was expected (Fig. 3), with the incorporation of Ni and Mo by one-pot or impregnation, the specific surface area and porous volume of the resultant solids decreased significantly and the decrease was more pronounced for the catalyst precursors prepared by impregnation (Table 1). These decreases can be mainly attributed to the partially blockage of the mesoporous system of the supports by the Mo and Ni species. On the other hand, in comparison with the others studied catalysts (Table 1), the impregnated NiMo(ox)/SiTi and NiMo(ox)/SiZr catalyst precursors presented very low pore volume. Here it must be considered that the cited catalyst precursors underwent two calcination steps. Besides the Mo and Ni oxides formation inside the mesopores, the heat treatments could also have led to a Si-Ti or Si-Zr structure collapse, thus strongly diminishing the pore volume.

In order to obtain more information related with the coordination and aggregation state of the Ni and Mo species, UV–vis DRS spectra of the pure mixed supports calcined at 550 °C, pure zirconia prepared by sol-gel and commercial titania P25 (Fig. 4) were recorded and compared to the ones of the supported NiMo oxides (Fig. 5). In the spectra of the commercial TiO_2 P25 (Fig. 4a), it can be observed an absorption band at 230 nm and other two absorption bands at 280 and 325 nm that correspond to the ligand-to-metal charge transfer $O_2 \rightarrow Ti^{4+}$. The absorption band at ca. 230 nm corresponds to isolated Ti atoms in tetrahedral (T_d) coordination and the absorption bands at ca. 280 nm and at Exhibits 330 nm with an

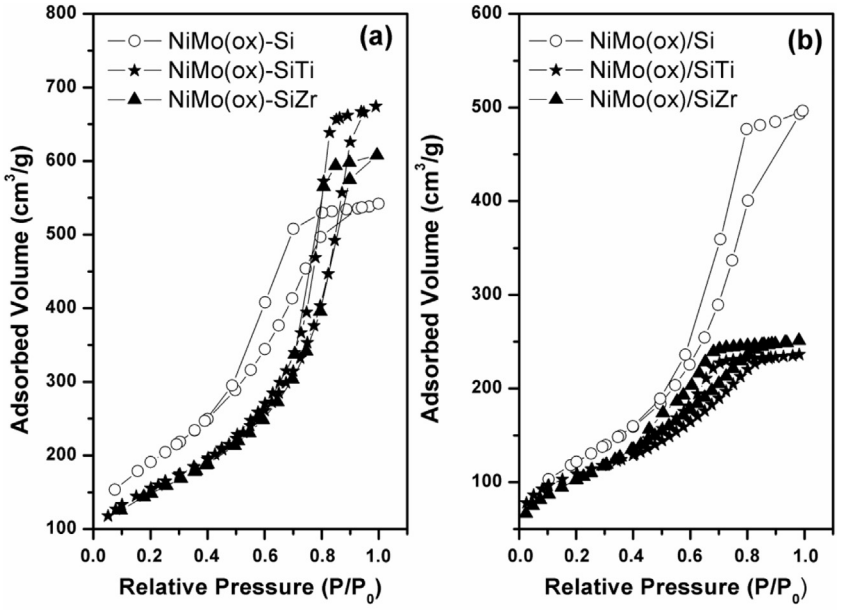

Fig. 3. N_2 adsorption-desorption isotherms of the supported NiMo oxides prepared by: (a) one-pot; (b) wet impregnation.

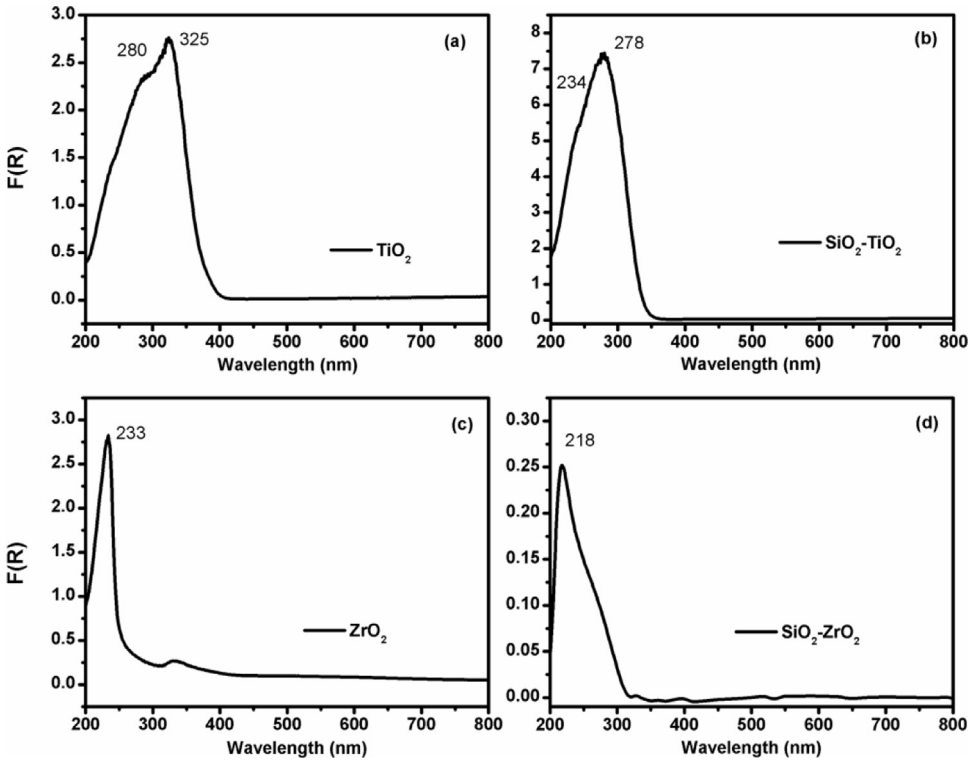

Fig. 4. UV–vis DRS spectra of: (a) silica-titania; (b) silica-zirconia; (c) P25 commercial titania; (d) tetragonal zirconia.

absorption edge at 390 nm correspond to polymerized octahedral (O_h) titanium species (Ti–O–Ti clusters) [11,25,58].

No absorption arises from silica, which is transparent in this region of the UV–vis spectrum (not shown). Nevertheless, the silica-titania mixed oxide (Fig. 4b) shows an absorption band at 234 nm, which is assigned to the ligand-to-metal charge-transfer between the ligand O^{2-} and titanium (IV) ion, corresponding to structural Ti^{4+} with tetrahedral coordination, and an absorption band at 278 nm corresponding to octahedral Ti, probably in a Ti-O-Ti-O-Si type structure. These bands clearly show that the most of the titanium (IV) was incorporated into the silica structure [52,59]. The UV–vis DRS spectrum of the silica-titania does not show any absorption from 330 to 400 nm, characteristic of Ti in anatase crystal structure, which reinforces the idea that most of Ti^{4+} ions were incorporated into the silica framework [11,59].

The UV–vis spectra of the pure zirconia (Fig. 4c) shows an absorption band at 230 nm, which is related to the transfer of the ligand to metal in Zr-O-Zr type bonds [11]. In the UV–vis DRS spectra of the silica-zirconia (Fig. 4d), it can be observed two absorption bands at 218 nm and a shoulder at 270 nm. The former is related

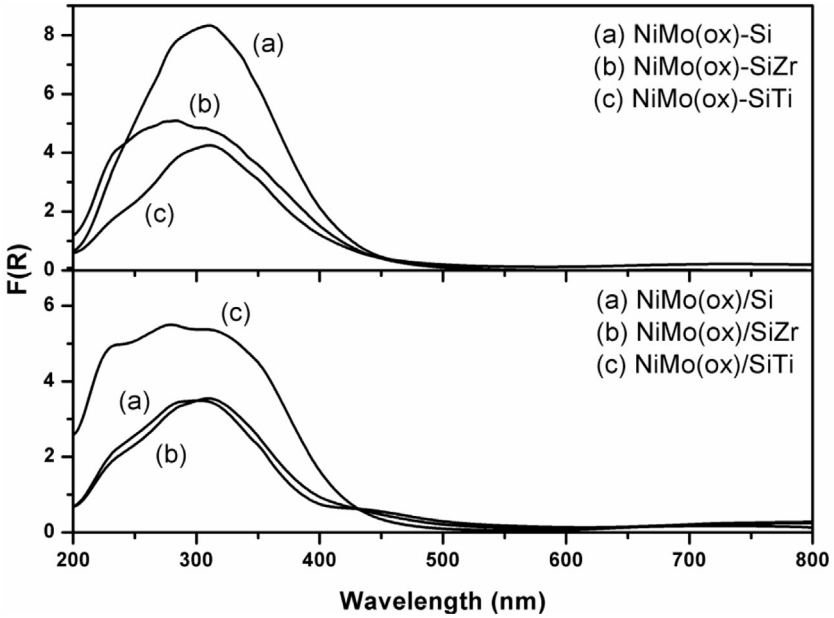

Fig. 5. UV–vis DRS spectra of the NiMo oxides supported on: (a) silica; (b) silica-zirconia; (c) silica-titania.

to the electronic transition of the ligand O^{2-} to Zr^{4+} in tetrahedral coordination [60]. This band is an evidence that Zr is well dispersed in the silica framework. The shoulder at 270 nm is probably associated with an electron transfer from the ligand to the metal in Si-O-Zr type bonds [60,61].

From the literature data, the UV–vis DRS spectrum of supported Mo oxide generally shows absorption bands between 200 and 400 nm [24], which correspond to Mo^{6+} ions with electronic configuration d^0, originated from the electronic transition of the valence level to the conduction level, a phenomenon which is attributed to the electron transfer from the ligand to metal ($O^{2-} \rightarrow Mo^{6+}$) [62]. The position of these absorption bands depends on the molybdenum coordination and degree of agglomeration. Isolated molybdate species with tetrahedral coordination (T_d) exhibit absorption bands between 220 and 280 nm [24], while species with octahedral (O_h) absorb in a wide range of wavelength where the maximum of the absorption band depends on the state of agglomeration of Mo^{6+} O_h species. Polymolybdate with octahedral coordination (MoO_3) have absorption bands between 300 and 330 nm and, with the increasing dispersion of octahedral Mo species, the absorption band shifts to lower wavelengths between 280 and 300 nm [11,63,64]. Thus, the spectra of the supported NiMo oxides (Fig. 5) show the presence of a mixture of Mo^{6+} ions species in tetrahedral (T_d) and octahedral coordination (O_h). However, the proportion of different types of Mo species changes with the support composition. The spectra of the NiMo(ox)-Si and NiMo(ox)-SiTi samples show a less intense UV–vis absorption band between 220 and 240 nm (Mo^{6+} T_d) and a more intense absorption band at around 300 and 330 nm (Mo^{6+} O_h), indicating the formation of more polymeric molybdenum species. An opposite trend occurred in the NiMo(ox)-SiZr sample, in which an increase in the intensity of the absorption band of Mo species in tetrahedral coordination (220–240 nm) is observed, which is a good evidence that the Mo species are more dispersed. Compared with the NiMo(ox)-SiTi sample, the NiMo(ox)/SiTi one also showed an intense absorption band at 230 nm ($Mo^{6+}T_d$) indicating that Mo in this sample prepared by impregnation is well dispersed on the SiTi support. Only in the spectra of samples NiMo(ox)/Si and NiMo(ox)/SiZr (Fig. 5) it was observed a well-defined absorption band at 450 nm that is related to octahedral Ni^{2+} [24,52,56].

Table 2
H_2 consumption of the supported NiMo oxides during the H_2-TPR analyses.

Sample	Reduction Peaks			H_2 Consumption (mol/g_{Mo})
NiMo(ox)-Si	388	458	–	0.031
NiMo(ox)-SiTi	397	458	797	0.028
NiMo(ox)-SiZr	374	503	–	0.028
NiMo(ox)/Si	378	426	598	0.027
NiMo(ox)/SiTi	378	426	598	0.026
NiMo(ox)/SiZr	370	426	598	0.024

The H_2-TPR profiles for the NiMo catalyst precursors are shown in Fig. 6 and Table 2 displays the H_2 consumption data, whose values are satisfactorily close to the theoretical ones. As it can be seen, the H_2-TPR profile of the precursor NiMo(ox)-Si exhibits a main reduction peak at 388 °C with a shoulder at 467 °C and a low-intensity broad peak in the high-temperature region (600 to 900 °C). The hydrogen consumption at temperatures lower than 500 °C can be ascribed to the reduction steps of octahedrally coordinated molybdenum species (Mo^{6+} to Mo^{4+}) weakly bonded with the silica surface and also to the reduction of Ni species; above 500 °C occurs the reduction of Mo^{4+} to Mo^0 [65]. The H_2 consumption at temperatures higher than 600 °C is attributed to the reduction of tetrahedral coordinated Mo species in strong interaction with the support [66]. In comparison with the NiMo(ox)-Si sample, the sample NiMo(ox)/Si prepared by impregnation shows a very similar reduction profile (Fig. 6), which demonstrates that irrespective of the preparation procedure, the resultant nature and dispersion of the silica supported NiMo species were very similar.

In comparison with the H_2-TPR profile of the NiMo(ox)-Si, the H_2-TPR profile of the NiMo(ox)-SiTi (Fig. 6) clearly shows that titanium incorporation into the silica framework led to a slight increase in the reduction temperatures of Mo. The increase of temperatures in the first reduction step could be also consequence of the reduction of octahedral coordinated Ni^{2+} ions in $NiTiO_3$-like structures [65]. This increase in the reduction temperatures was also observed by Gutiérrez et al. [24] in the reduction behavior of supported NiMo oxides on Ti-SBA-15, which was attributed to a higher interaction of Ni and Mo with titanium. The higher inter-

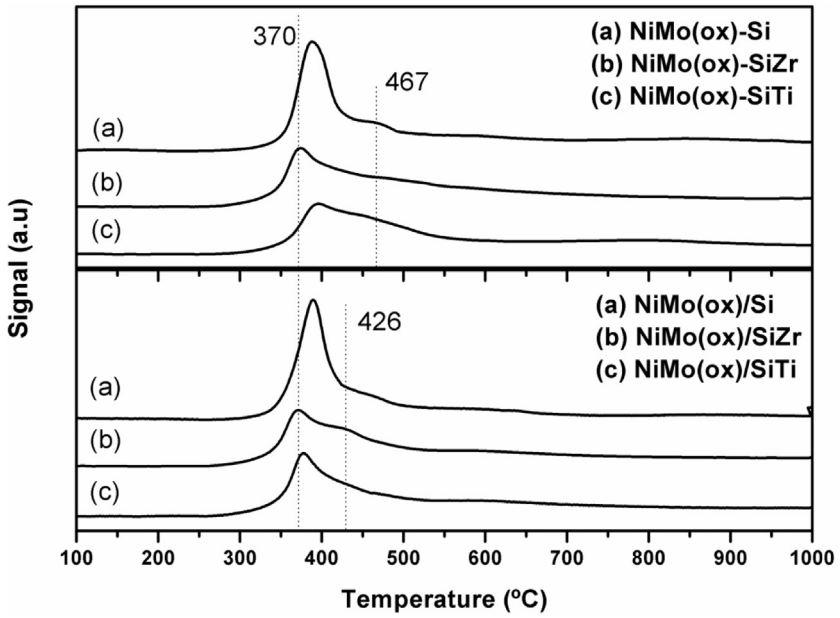

Fig. 6. H_2-TPR profiles of the precursor NiMo oxides supported on: (a) silica; (b) silica-titania; (c) silica-zirconia.

action of Mo with the SiTi support can be better evidenced at temperatures higher than 700 °C corresponding to the reduction of tetrahedral molybdenum species in strong interaction with the support. On the other hand, the H_2-TPR profile for the impregnated NiMo(ox)/SiTi sample (Fig. 6) shows lower Mo reduction temperatures with peaks at 378, 426 °C and 589 °C mainly attributed, respectively, to the reduction of Mo^{6+} to Mo^{4+}, Mo^{4+} to Mo^0 and the reduction of tetrahedral Mo previously discussed [66]. The higher Ni and Mo reduction temperatures in the H_2-TPR profile of the SiTi supported NiMo oxides suggest that the Ni and Mo species resultant from the one-pot synthesis interact more strongly with the SiTi support than those resultant from impregnation.

Opposite behavior was observed for the NiMo oxides supported on SiZr, where a decrease in the Mo reduction temperatures (Fig. 6), with reduction peaks at 370 °C (Mo^{6+} to Mo^{4+}) and a broad peak at about 458 °C (Mo^{4+} to Mo^0) was observed. This profile indicates an easier reduction of octahedral molybdenum when supported on a SiZr support. In addition, it must be mentioned that the H_2-TPR profile of the NiMo(ox)-SiZr sample also shows a decrease in the hydrogen consumption at temperatures higher than 600 °C that correspond to the reduction of Mo (T_d) species (600 to 800 °C), indicating a smaller formation of those Mo(T_d) species, which are more difficult to reduce [13,24,52,56].

As discussed above, the H_2-TPR profiles of the NiMo catalyst precursors (Fig. 6) prepared by conventional impregnation or by the one-pot methodology only showed some differences in the Ni or Mo reduction temperatures as a function of their interaction with the incorporation of Ti or Zr in the silica framework. Those profiles do not show any important difference related with the used preparation procedure despite higher Mo reduction temperatures should be expected for the NiMo catalyst precursors prepared by one-pot. This result is consistent with data published by other authors [17,30,38,43], who supported their findings based on the formation of highly dispersed Mo particles. As evidenced by XRD (Fig. 1) and UV–vis DRS (Fig. 5), the NiMo catalysts prepared by the discussed methods showed very similar characteristic related with high dispersion and similar nature of the formed Mo species.

3.2. Sulfided catalysts

High resolution TEM images of the sulfided NiMoS-Si catalyst are displayed in Fig. 7 and Fig. S1. As can be seen the pictures clearly show typical fringes of MoS_2 slabs with 0.61 nm interplanar distance that are characteristics of the (002) atomic planes of MoS_2 slabs [67,68]. Based on HRTEM images published by Li et al. [67] and Hyden et al. [68] and other authors [67–71], the most of the MoS_2 slabs in Fig. 7 could perhaps be assigned as edge-bonded oriented. These slabs present lengths between 2.5 and 6.8 nm and are constituted by two to seven atomic layers.

Fig. 8 shows the HRTEM images of the sulfided NiMoS/Si catalyst prepared by impregnation and it can be observed that the MoS_2 slabs also show interplanar distances of 0.61 nm that are characteristics of the (002) atomic planes. However, it can be seen that there is less formation of edge-bonded oriented MoS_2 slabs when compared to the NiMoS-Si one-pot prepared catalyst (Fig. 7). On the other hand, the images in Fig. 8b and Fig. 8c also show slabs with interplanar atomic distances of 0.26 nm of the (100) atomic planes that can be attributed to the top view of MoS_2 structures that could perhaps be basal-bonded as suggested in earlier studies [67–71]. Pawelec et al. [70] described that the edge sites of the edge-bonded MoS_2 slabs, which are perpendicular to the support surface, might have a lower metal–support interaction in comparison with the MoS_2 slabs basally bonded with the support surface. That lower interaction of the edge-bonded MoS_2 with the support could also support the H_2-TPR results (Table 2), where the NiMo(ox)-Si catalyst prepared by one-pot presented only two Mo reduction peaks and it was completely reduced at lower temperatures. The assignment that the formation of the edge-bonded MoS_2 slabs on the NiMoS-Si catalyst is superior to that on the NiMoS/Si one can be attributed to the random distribution of the ammonium heptamolybdate in the bulk formed gel that generated its catalyst precursor.

Fig. S2 presents HRTEM images of the sulfided NiMoS-SiTi catalyst prepared by the one-pot methodology. As it can be seen, the images show only few typical fringes of MoS_2 slabs, indicating that the silica-titania support does not favor the formation of highly

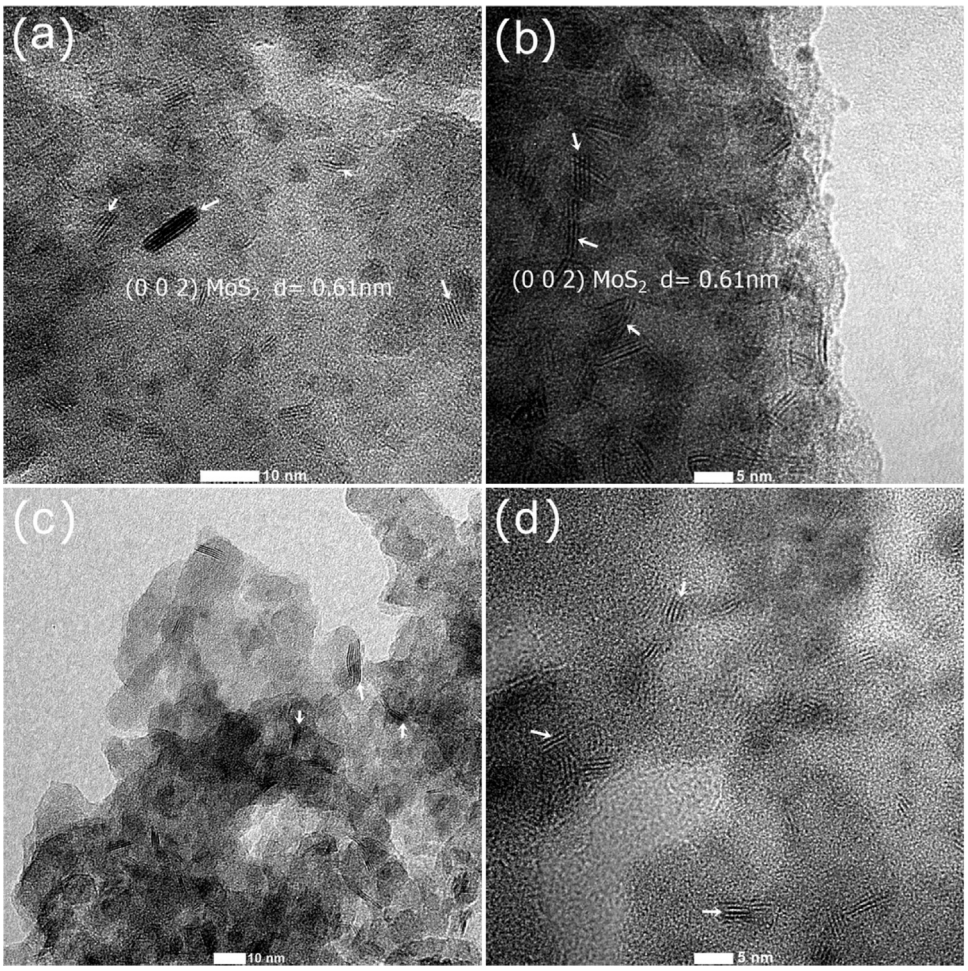

Fig. 7. (a); (b); (c) and (d): HRTEM images of the sulfided NiMoS-Si catalyst whose precursor was one-pot prepared.

crystalline MoS_2 during the sulfidation process under the used conditions.

Fig. 9 shows the Raman spectra of the studied NiMo catalysts in the sulfided-form using commercial bulk MoS_2 as reference. The Raman spectrum of the bulk MoS_2 shows two main Raman-active modes, the $E_{2g}{}^1$ (393 cm^{-1}) and A_{1g} (420 cm^{-1}). The $E_{2g}{}^1$ mode represents an in-plane vibration, and the A_{1g} one corresponds to an out-of-plane lattice expansion [72–74]. The Ramam spectra of the studied sulfided catalysts show these two Raman modes, thus corroborating the formation of the molybdenum sulfide. In Fig. 9, it is also possible to observe in the spectra of the sulfided catalysts an increase in the frequency of the two mentioned vibration modes (blue shift), indicating an interaction of the sulfide with the support that partially suppress the vibration of the MoS_2 atoms [72,75]. Fig. 9 also shows that there is a difference in the intensity of the vibration modes of the sulfided catalysts compared to the bulk MoS_2, which is related to the number of layers of the formed molybdenum sulfide [76]. The Raman spectrum of the NiMoS/Si catalyst showed the highest intensity compared to the others with a value close to the bulk MoS_2, thus indicating the formation of multi-layers of MoS_2 on its surface. As it can be evidenced in Fig. 9, all the catalysts prepared by impregnation showed vibration modes of higher intensity when compared with the samples prepared by the one-pot methodology.

Comparing the HRTEM images of the NiMoS-Si (Fig. 7), NiMoS/Si (Fig. 8) and NiMoS-SiTi (Fig. S2) catalysts and their respective Raman spectra (Fig. 9), it is possible to observe the evolution of the intensities of the vibration modes. The Raman spectrum of the NiMoS-SiTi catalyst (Fig. 9) shows low intensity and the HRTEM images (Fig. S2), only little formation of molybdenum sulfide. On the other hand, the Raman spectra of the NiMoS-Si and NiMoS/Si catalysts (Fig. 9) show vibration modes with higher intensity and their respective HRTEM images (Figs. 7 and 8, respectively) coherently show important formation of MoS_2. Thus, as the HRTEM images of the sample prepared by impregnation (NiMoS/Si) showed the formation of higher and more defined particles of MoS_2 (Fig. 8), its Raman spectrum consequently was the most intense.

3.3. Catalytic activity

As shown in Table 3, the HDS of thiophene at 300 °C on the studied catalysts mainly resulted in the formation of 1-butene, *n*-butane (derived from the hydrogenation of butenes [64]), *trans*-2-butene and *cis*-2-butene with no important differences in the selectivity. As it is well known, there are many proposed mechanisms for the HDS reaction [53]. Particularly for thiophene an accepted general mechanism for the sulfur removal [77], begins with the hydrogenation of the unsaturated bond of the thiophene ring, followed by the cleavage of the C-S linkage in two steps: the formation of butadiene, an intermediate for the subsequent formation of the other products. The hydrogenation of butadiene for the formation of butene-1 and the consecutive steps to the formation of the *cis*-and *trans*-butene-2 isomers occur quickly [77].

Fig. 10 shows the specific activity of the sulfide NiMo catalysts that was calculated using Eq. (2). As can be seen the NiMoS-Si and NiMoS-SiZr one-pot prepared catalysts and the

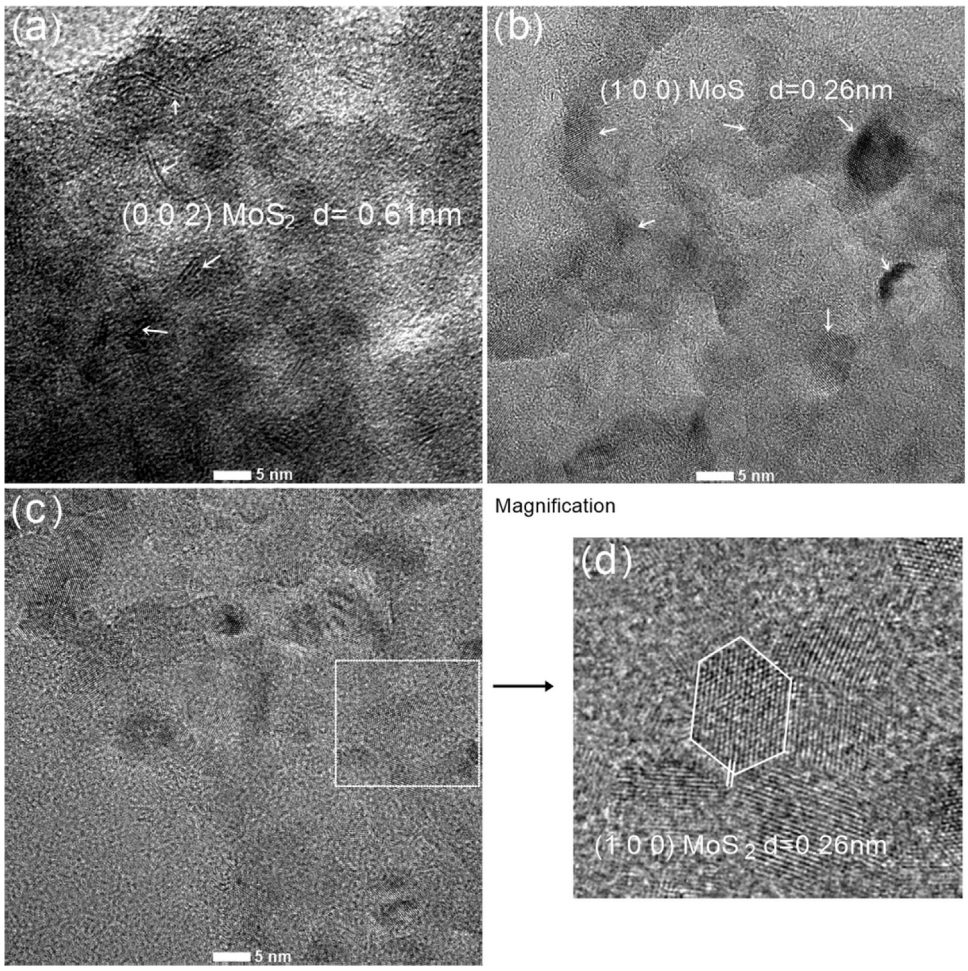

Fig. 8. (a); (b); and (c): HRTEM images of the sulfided NiMoS/Si catalyst whose precursor was prepared by impregnation; (d) magnification of image (c).

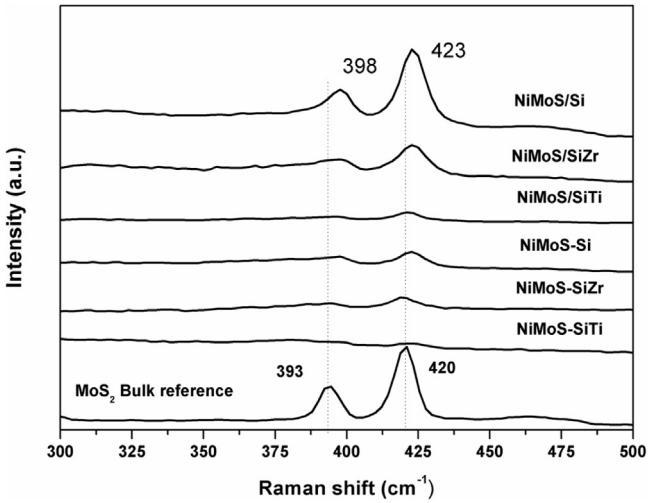

Fig. 9. Raman spectra of the studied supported NiMoS catalysts and of a sample of bulk MoS_2.

NiMoS/Si ones, impregnated prepared, present highest values of specific activity in temperatures higher than 260 °C. The following order of specific activity is observed: NiMoS-Si > NiMoS-SiZr > NiMoS/Si > NiMoS/SiTi > NiMoS/SiZr > NiMoS-SiTi. From Fig. 10 it is interesting to notice that the NiMoS-Si and NiMoS-SiZr catalysts show higher specific activity than a reference sulfided

Table 3
Thiophene conversion[a] and reaction product selectivity[b] obtained on the studied NiMoS catalysts at 300 °C (1 atm; 100 mg of catalyst; feed of 8.2% (V/V) of thiophene in H_2).

Sample	Conversion (%)	Selectivity (%)			
		1-butene	*n*-butane	*c*-2-buteno	*t*-2-buteno
NiMoS-Si	11,4	19,7	2,2	47	31
NiMoS-SiTi	6,6	19,5	2,3	47	31,2
NiMoS-SiZr	11,5	19,4	2,8	46,5	31,2
NiMoS/Si	11	20,2	1,0	48	30,6
NiMoS/SiTi	9,8	19,7	3,4	46	31
NiMoS/SiZr	9,9	20	2,8	46	31,1

[a] Calculated from Eq. (1).
[b] Calculated as $S_i = 100\,(x_{iDS}/\sum x_{iDS})$, where x_{iDS} is the molar fraction of the desulfurized product.

commercial HDS catalyst (NiMoPS/alumina in Table 1) and those ones prepared by wet impregnation. As can be seen from Table 1, the commercial sample presents nearly of 90% more active species than the NiMoS-Si and NiMoS-SiZr samples. Considering that the commercial catalyst precursor was sulfided under the same conditions, the used time might have been insufficient to sulfide all of their active species and this could be the reason of its unexpectedly low activity.

In Fig. 10 it is also observed that there is no important difference between the SA values of the NiMoS-Si and NiMoS-SiZr catalysts that can be explained from the XRD and UV–vis DRS data of the last that evidenced a lack of detectable crystalline zirconia clusters

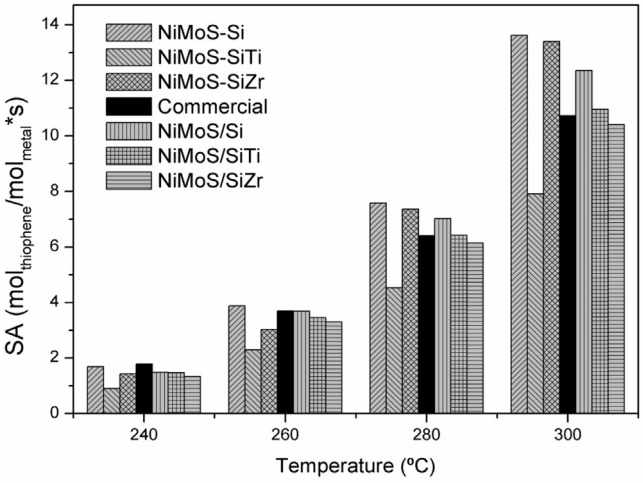

Fig. 10. Specific activity (SA) of the studied supported NiMoS catalysts and of a commercial NiMoPS/alumina catalyst as a function of the reaction temperature during thiophene HDS at 240, 260, 280 and 300 °C (1 atm; 100 mg of catalyst; feed of 8.2% (V/V) of thiophene in H_2).

as consequence of its high distribution into the silica framework [19]. On the other hand, the incorporation of Ti into the silica support led to a thiophene HDS activity loss, as it can be observed from the values of SA of the NiMoS-SiTi and NiMoS/SiTi catalysts when are respectively compared with the values of the NiMoS-Si and NiMoS/Si ones (Fig. 10). This decrease in the activity may be explained by the more interaction between Ni and Mo with the silica-titania support, as was also noticed by Olguin et al. [78], who studied NiMo catalysts supported on alumina-titania. Those authors explained that during sulfidation of the catalyst precursors due to the strong interaction of Mo with the titanium incorporated in the alumina framework simultaneously occurs the formation of MoS_2 and inactive HDS MoO_2, which is hardly sulfided. Corroborating this lower MoS_2 formation, the HRTEM images of the NiMoS-SiTi catalyst (Fig. S2) do not clearly show the formation of MoS_2 slabs in some extension. The effect of the Ti incorporation into the silica framework was smaller in the catalyst NiMoS/SiTi prepared by wet impregnation, which showed from the H_2-TPR results (Fig. 6) lower interaction of the active species with the support.

From Fig. 10 it is also possible to observe a tendency to an increase of the specific activity of the NiMoS catalysts with the increase of specific surface area of their respective precursors (Table 1). Nevertheless, even the precursor of the NiMoS-SiTi catalyst has showed higher specific surface area (Table 1), it presented lower specific activity than the NiMoS/SiTi one. That behavior can be explained as result of the higher interaction of their active species with the support as discussed from its H_2-TPR data (Fig. 6).

In fact, the interaction of the active species with the support can explain the tendency for the obtained specific activity of the catalysts (Fig. 10), where active species having lower interaction with the support had higher specific activity. Moreover, the more active catalysts showed more intense bands of molybdenum sulfide in the Raman spectra (Fig. 9) and, as observed in the TEM images, more formation of MoS_2 slabs in the case of the NiMoS-Si and NiMoS/Si catalysts (Fig. 7 and 8, respectively).

Moreover, as it was discussed before, the HRTEM images of the NiMoS-Si prepared by one-pot (Fig. 7) allowed to assign the formation of more molybdenum sulfide slabs with edge-bonded orientation than those ones formed on the NiMoS/Si, which were assigned as more basal-bonded oriented (Fig. 8). It has been proposed in the literature [9,79,80] that the MoS_2 edge-bonded oriented slabs present higher activity than the basal-bonded oriented ones, which could perhaps also explain the superior activity of the NiMoS-Si sample (Fig. 10). Araki et al. [9] using NO chemisorption data estimated the number of HDS active catalytic sites and verified that the catalysts having more edge-bonded oriented MoS_2 slabs presented a higher value of NO uptake than catalysts having a higher number of basal-bonded MoS_2 slabs. Araki et al. [9], also observed that the activity on the basal bonded MoS2 slabs increased with the increase of the sulfidation temperature, which was attributed to a decrease in the electronic interaction between the basal-bonded MoS2 slabs and the support, as consequence of the transformation of single-layered MoS2 slabs to multilayered ones.

Based on several studies, Araki et al. [9] and Shimada [80] concluded that the catalytic performance of Co(Ni)–Mo–S structures also depends on the orientation of the MoS_2 slabs on the support, because the upper edge sites of the "edge-bonded" MoS_2 slabs, that are perpendicular to the support surface, have weaker electronic interaction with the support than the single "basal-bonded" layered MoS_2 slabs, which have high interaction with the support, forming Co(Ni)-Mo-S Type I catalysts. Furthermore, the upper edge sites in the edge-bonded MoS_2 slabs or in the multilayered basal-bonded ones have less steric hindrance than either the edge sites of the basal-bonded single-layered MoS_2 slabs or the edge sites of the bottom layers of the basal-bonded multilayered MoS_2 slabs.

Based on the obtained results and the discussion above, it can be concluded that the higher HDS catalytic activity of the silica supported NiMoS catalyst prepared by the one-pot methodology (NiMoS-Si) was consequence by the formation of the more active edge-bonded MoS_2 slabs. On the other hand, based on the Raman (Fig. 9) and HRTEM (Fig. 8) results, the considerable HDS activity of the impregnated NiMoS catalyst supported on silica (NiMoS/Si), may be attributed to the formation of well-active Type II HDS catalysts on multilayer basal-bonded MoS_2 slabs [9,80]. At this point, it is important to emphasize that according to several studies [81–85], the high HDS activity of the edge located MoS_2 active sites results from the strong promoting effect of Ni (or Co) that are incorporated in the edges of the MoS_2 slabs forming the well-described Ni-Mo-S or Co-Mo-S type structures.

The studied NiMoS-Si and NiMo-SiZr catalysts with high SA values (Fig. 10) put in evidence that the used one-pot synthesis procedure to prepare the catalyst precursor leads to highly active HDS catalysts with the important advantages in reducing the preparation time, energy consumption and, consequently, reducing the catalyst production cost.

4. Conclusions

HDS precursor NiMo catalysts supported on SiO_2, SiO_2-TiO_2 or SiO_2-ZrO_2 with high specific surface area were prepared by a one-pot procedure or by wet impregnation adding a chelating agent into the respective salts solution. XRD, H_2-TPR and UV–vis DRS data evidenced that both methods led to catalysts precursors with Mo oxide highly disperse on the supports with only little differences between them caused by the incorporation of Ti or Zr into the amorphous silica framework. After the precursor sulfidation, the HRTEM and Raman analyses showed the effective formation of MoS_2 slabs on the support. For the NiMoS-Si catalyst, whose precursor was one-pot prepared, the HRTEM images evidenced high formation of edge-bonded oriented MoS_2 slabs, and for the NiMoS/Ti one the HRTEM images indicated more formation of slabs basal-bonded oriented. In the NiMoS-SiTi catalyst, the obtained HRTEM images did not show consistent formation of MoS_2 slabs which was attributed to the strong interaction between Mo and Ti incorporated into the silica framework.

Coherent with the formation of MoS_2 slabs and the important promoting effect of Ni in the HDS activity of Mo, all the prepared cat-

alysts were active in the HDS of thiophene, with those supported on SiO_2 or SiO_2-ZrO_2 and whose precursor was one-pot prepared being the most actives. Because of the lower formation of MoS_2 slabs on the NiMoS-SiTi catalyst it presented the lowest HDS specific activity. No observable effect was noticed in that activity related with the incorporation of Zr into the silica framework that was attributed to the lack of formation of crystalline zirconia clusters as consequence of its high distribution into the silica framework.

Taking into consideration the Raman and HRTEM data, the highest specific activity of the NiMoS-Si catalyst was clearly related with the predominant formation of the more active edge-bonded MoS_2 slabs. Also based on Raman and HRTEM results, the considerable HDS activity obtained on the impregnation prepared NiMoS catalyst supported on SiO_2 was attributed to the formation of the well-active Type II HDS catalysts on multilayer basal-bonded MoS_2 slabs.

The studied NiMoS-Si and NiMo-SiZr with high SA values put in evidence that the used one-pot synthesis methodology to prepare the catalyst precursor leads to highly active HDS catalysts with the important advantages of reducing the preparation time, energy consumption and consequently reducing the catalyst production cost.

Acknowledgements

The authors are grateful to the Brazilian Founding Agencies CAPES and CNPq, and Petrobras Brazil for the financial support.

Appendix A. Supplementary data

Supplementary data associated with this article can be found, in the online version, at http://dx.doi.org/10.1016/j.apcata.2016.09.019.

References

[1] C. Song, Catal. Today 86 (2003) 211–263.
[2] S.K. Bej, S.K. Maity, U.T. Turaga, Energy Fuels 18 (2004) 1227–1237.
[3] H. Song, J. Wang, Z. Wang, H. Song, F. Li, Z. Jin, J. Catal. 311 (2014) 257–265.
[4] R. Huirache-Acuña, T.A. Zepeda, E.M. Rivera-Muñoz, R. Nava, C.V. Loricera, B. Pawelec, Fuel 149 (2015) 149–161.
[5] M.A. Guzmán, R. Huirache-Acuña, C.V. Loricera, J.R. Hernández, J.N. Díaz de León, J.A. de los Reyes, et al., Fuel 103 (2013) 321–333.
[6] A. Sampieri, S. Pronier, J. Blanchard, M. Breysse, S. Brunet, K. Fajerwerg, C. Louis, G. Perot, Catal. Today 107–08 (2005) 537–544.
[7] I.V. Babich, J.A. Moulijn, Fuel 82 (2003) 607–631.
[8] G.M. Dhar, B.N. Srinivas, M.S. Rana, M. Kumar, S.K. Maity, Catal. Today 86 (2003) 45–60.
[9] Y. Araki, K. Honna, H. Shimada, J. Catal. 207 (2002) 361–370.
[10] G. Lara, J. Escobar, J.A. De Los Reyes, M.C. Barrera, J.A. Colin, F.R. Murrieta, Can. J. Chem. Eng. 83 (2005) 685–694.
[11] T. Klimova, O. Gutiérrez, L. Lizama, J. Amezcua, Micropor. Mesopor. Mater. 133 (2010) 91–99.
[12] H. Shang, C. Liu, Y. Xu, J. Qiu, F. Wei, Fuel Process. Technol. 88 (2007) 117–123.
[13] S.K. Maity, M.S. Rana, B.N. Srinivas, S.K. Bej, G.M. Dhar, T. Rao, J. Mol. Catal. A-Chem. 153 (2000) 121–127.
[14] A.K. Datye, S. Srinivasan, L.F. Allard, C.H.F. Peden, J.R. Brenner, L.T. Thompson, J. Catal. 158 (1996) 205–216.
[15] M.S. Rana, B.N. Srinivas, S.K. Maity, G.M. Dhar, T. Rao, Stud. Surf. Sci. Catal. 127 (1999) 397–400.
[16] S. Damyanova, L. Petrov, M.A. Centeno, P. Grange, Appl. Catal. A-Gen. 224 (2002) 271–284.
[17] E.P. Baston, A.B. França, A.V.d.S. Neto, E.A. Urquieta-González, Catal. Today 246 (2015) 184–190.
[18] J. Ramirez, P. Rayo, A. Gutierrez-Alejandre, J. Ancheyta, M.S. Rana, Catal. Today 109 (2005) 54–60.
[19] M.S. Rana, S.K. Maity, J. Ancheyta, G.M. Dhar, T. Rao, Appl. Catal. A-Gen. 268 (2004) 89–97.
[20] M.S. Rana, S.K. Maity, J. Ancheyta, G.M. Dhar, T. Rao, Appl. Catal. A-Gen. 253 (2003) 165–176.
[21] S. Damyanova, P. Grange, B. Delmon, J. Catal. 168 (1997) 421–430.
[22] J.M. Herrera, J. Reyes, P. Roquero, T. Klimova, Micropor. Mesopor. Mater. 83 (2005) 283–291.
[23] T.A. Zepeda, J.L.G. Fierro, B. Pawelec, R. Nava, T. Klimova, G.A. Fuentes, T. Halachev, Chem. Mater. 17 (2005) 4062–4073.
[24] O.Y. Gutierrez, G.A. Fuentes, C. Salcedo, T. Klimova, Catal. Today 116 (2006) 485–497.
[25] J.A. Mendoza-Nieto, I. Puente-Lee, C. Salcedo-Luna, T. Klimova, Fuel 100 (2012) 100–109.
[26] R.D. Gonzalez, T. Lopez, R. Gomez, Catal. Today 35 (1997) 293–317.
[27] F. Dumeignil, K. Sato, M. Imamura, N. Matsubayashi, E. Payen, H. Shimada, Appl. Catal. A: Gen. 315 (2006) 18–28.
[28] A.M. Venezia, V. La Parola, G. Deganello, D. Cauzzi, G. Leonardi, G. Predieri, Appl. Catal. A: Gen. 229 (2002) 261–271.
[29] P. Schacht, G. Hernandez, L. Cedeno, J.H. Mendoza, S. Ramirez, L. Garcia, J. Ancheyta, Energy Fuel 17 (2003) 81–86.
[30] E.P. Baston, E.A. Urquieta-Gonzalez, Stud. Surf. Sci. Catal. 175 (2010) 671–674.
[31] A.J. Duan, R.L. Li, G.Y. Jiang, J.S. Gao, Z. Zhao, G.F. Wan, D.Q. Zhang, W.Q. Huang, K.H. Chung, Catal. Today 140 (2009) 187–191.
[32] V. La Parola, G. Deganello, S. Scirè, A.M. Venezia, J. Solid State Chem. 174 (2003) 482–488.
[33] M.C. Barrera, J. Escobar, J.A. de los Reyes, M.A. Cortes, M. Viniegra, A. Hernandez, Catal. Today 116 (2006) 498–504.
[34] L.L. Hench, J.K. West, Chem. Rev. 90 (1990) 33–72.
[35] D.A. Ward, E.I. Ko, Ind. Eng. Chem. Res. 34 (1995) 421–433.
[36] J.B. Miller, E.I. Ko, Catal. Today 35 (1997) 269–292.
[37] G. Liu, Y. Liu, G. Yang, S.Y. Li, Y.H. Zu, W.X. Zhang, M.J. Jia, J. Phys. Chem. C 113 (2009) 9345–9351.
[38] R. Takahashi, S. Sato, T. Sodesawa, M. Suzuki, N. Ichikuni, Micropor. Mesopor. Mater. 66 (2003) 197–208.
[39] J.B. Pang, K.Y. Qiu, Y. Wei, J. Non-Cryst. Solids 283 (2001) 101–108.
[40] O.V. Klimov, A.V. Pashigreva, M.A. Fedotov, D.I. Kochubey, Y.A. Chesalov, G.A. Bukhtiyarova, A.S. Noskov, J. Mol. Catal. A-Chem. 322 (2010) 80–89.
[41] N. Rinaldi, T. Kubota, Y. Okamoto, Appl. Catal. A: Gen. 374 (2010) 228–236.
[42] J. Escobar, M.C. Barrera, J.A. de los Reyes, J.A. Toledo, V. Santes, J.A. Colin, J. Mol. Catal. A: Chem. 287 (2008) 33–40.
[43] A.V.d. Silva Neto, P.P.C. Sartoratto, M.C.d. Rangel, Stud. Surf. Sci. Catal. 167 (2007) 475–480.
[44] M.Á. Calderón-Magdaleno, J.A. Mendoza-Nieto, T.E. Klimova, Catal. Today 220–222 (2014) 78–88.
[45] P.A. Nikulshin, A.V. Mozhaev, A.A. Pimerzin, V.V. Konovalov, A.A. Pimerzin, Fuel 100 (2012) 24–33.
[46] R. Cattaneo, T. Shido, R. Prins, J. Catal. 185 (1999) 199–212.
[47] R. Cattaneo, F. Rota, R. Prins, J. Catal. 199 (2001) 318–327.
[48] W. Lai, L. Pang, J. Zheng, J. Li, Z. Wu, X. Yi, W. Fang, L. Jia, Fuel Process. Technol. 110 (2013) 8–16.
[49] R. Nava, A. Infantes-Molina, P. Castaño, R. Guil-López, B. Pawelec, Fuel 90 (2011) 2726–2737.
[50] H. Izutsu, P.K. Nair, K. Maeda, Y. Kiyozumi, F. Mizukami, Mater. Res. Bull. 32 (1997) 1303–1311.
[51] Z.G. Wu, Y.X. Zhao, D.S. Liu, Micropor. Mesopor. Mater. 68 (2004) 127–132.
[52] T.A. Zepeda, B. Pawelec, J.L.G. Fierro, A. Olivas, S. Fuentes, T. Halachev, Micropor. Mesopor. Mater. 111 (2008) 157–170.
[53] A. Wang, Y. Wang, T. Kabe, Y. Chen, A. Ishihara, W. Qian, P. Yao, J. Catal. 210 (2002) 319–327.
[54] T.A. Zepeda, B. Pawelec, J.L.G. Fierro, T. Halachev, J. Catal. 242 (2006) 254–269.
[55] T.A. Zepeda, Appl. Catal. A: Gen. 347 (2008) 148–161.
[56] O.Y. Gutierrez, D. Valencia, G.A. Fuentes, T. Klimova, J. Catal. 249 (2007) 140–153.
[57] R. Takahashi, S. Sato, T. Sodesawa, M. Kawakita, K. Ogura, J. Phys. Chem. B 104 (2000) 12184–12191.
[58] Z. Luan, E.M. Maes, P.A.W. van der Heide, D. Zhao, R.S. Czernuszewicz, L. Kevan, Chem. Mater. 11 (1999) 3680–3686.
[59] Z.Y. Wu, Y.F. Tao, Z. Lin, L. Liu, X.X. Fan, Y. Wang, J. Phys. Chem. C 113 (2009) 20335–20348.
[60] G. Yu, L. Zhu, X. Wang, J. Liu, D. Xu, Micropor. Mesopor. Mater. 130 (2010) 189–196.
[61] K. Chaudhari, R. Bal, T.K. Das, A. Chandwadkar, D. Srinivas, S. Sivasanker, J. Phys. Chem. B 104 (2000) 11066–11074.
[62] Z. Liu, Y. Chen, J. Catal. 177 (1998) 314–324.
[63] S. Higashimoto, Y. Hu, R. Tsumura, K. Iino, M. Matsuoka, H. Yamashita, Y.G. Shul, M. Che, M. Anpo, J. Catal. 235 (2005) 272–278.
[64] A.J. Duan, G.F. Wan, Z. Zhao, C.M. Xu, Y.Y. Zheng, Y. Zhang, T. Dou, X.J. Bao, K. Chung, Catal. Today 119 (2007) 13–18.
[65] J.C. Amezcua, L. Lizama, C. Salcedo, I. Puente, J.M. Dominguez, T. Klimova, Catal. Today 107–08 (2005) 578–588.
[66] T. Klimova, L. Pena, L. Lizama, C. Salcedo, O.Y. Gutierrez, Ind. Eng. Chem. Res. 48 (2009) 1126–1133.
[67] Y. Li, A. Li, F. Li, D. Liu, Y. Chai, C. Liu, J. Catal. 317 (2014) 240–252.
[68] T.F. Hayden, J.A. Dumesic, J. Catal. 103 (1987) 366–384.
[69] Y. Sakashita, T. Yoneda, J. Catal. 185 (1999) 487–495.
[70] B. Pawelec, P. Castaño, T.A. Zepeda, Appl. Surf. Sci. 254 (2008) 4092–4102.
[71] R. Prins, V.H.J. De Beer, G.A. Somorjai, Catal. Rev. 31 (1989) 1–41.
[72] H. Li, Q. Zhang, C.C.R. Yap, B.K. Tay, T.H.T. Edwin, A. Olivier, D. Baillargeat, Adv. Funct. Mater. 22 (2012) 1385–1390.
[73] I. Paradisanos, E. Kymakis, C. Fotakis, G. Kioseoglou, E. Stratakis, Appl. Phys. Lett. 105 (2014) 041108.
[74] K.G. Zhou, F. Withers, Y. Cao, S. Hu, G. Yu, C. Casiraghi, ACS Nano 8 (2014) 9914–9924.
[75] N. Kunisada, K.-H. Choi, Y. Korai, I. Mochida, K. Nakano, Appl. Catal. A: Gen. 276 (2004) 51–59.

[76] J.W. Park, H.S. So, S. Kim, S.-H. Choi, H. Lee, J. Lee, Y. Kim, J. Appl. Phys. 116 (2014) 183509.
[77] M.J.B. Souza, B.A. Marinkovic, P.M. Jardim, A.S. Araujo, A.M.G. Pedrosa, R.R. Souza, Appl. Catal. A: Gen. 316 (2007) 212–218.
[78] E. Olguin, M. Vrinat, L. Cedeño, J. Ramirez, M. Borque, A. López-Agudo, Appl. Catal. A: Gen. 165 (1997) 1–13.
[79] H. Topsøie, R. Candia, N.-Y. Topsøe, B.S. Clausen, H. Topsøe, Bull. Soc. Chim. Belg. 93 (1984) 783–806.
[80] H. Shimada, Catal. Today 86 (2003) 17–29.
[81] R. Candia, B.S. Clausen, H. Topsoe, J. Catal. 77 (1982) 564–566.
[82] H. Topsøe, Appl. Catal. A: Gen. 322 (2007) 3–8.
[83] P.G. Moses, B. Hinnemann, H. Topsoe, J.K. Norskov, J. Catal. 268 (2009) 201–208.
[84] S. Eijsbouts, Appl. Catal. A: Gen. 158 (1997) 53–92.
[85] S. Eijsbouts, L.C.A. van den Oetelaar, R.R. van Puijenbroek, J. Catal. 229 (2005) 352–364.